JOURNAL OF GEOPHYSICAL RESEARCH, VOL. 105, NO. A6, PAGES 12,907–12,917, JUNE 1, 2000

The temporal evolution of electron distributions and associated wave activity following substorm injections in the inner magnetosphere

Nigel P. Meredith, [1] Richard B. Horne, [2] Alan D. Johnstone, [1,3] and Roger R. Anderson [4]

Abstract. The temporal evolution of electron distributions and associated wave activity following substorm injections in the inner magnetosphere are investigated using data from the CRRES satellite. Equatorial electron distributions and concomitant wave spectra outside the plasmapause on the nightside of the Earth are studied as a function of time since injection determined from the auroral-electrojet index (AE). The electron cyclotron harmonic (ECH) wave amplitudes are shown to be very sensitive to small modeling errors in the location of the magnetic equator. They are best understood at the ECH equator, defined by the local maximum in the ECH wave activity in the vicinity of the nominal magnetic equator, suggesting that the ECH equator is a better measure of the location of the true equator. Strong ECH and whistler mode wave amplitudes are associated with the injected distributions and at the ECH equator, in the region $6.0 \leq L < 7.0$, exponential fits reveal wave amplitude decay time constants of 6.3 ± 1.2 and 4.6 ± 0.7 hours, respectively. Pancake electron distributions are seen to develop from injected distributions that are nearly isotropic in velocity space and, in this region, are seen to form on a similar timescale of approximately 4 hours suggesting that both wave types are involved in their production. The timescale for pancake production and wave decay is comparable with the average time interval between substorm events so that the wave-particle interactions are almost continually present in this region leading to a continual supply of electrons to power the diffuse aurora. In the region $3.8 \leq L < 6.0$ the timescale for wave decay at the ECH equator is 2.3 ± 0.6 and 1.1 ± 0.2 hours for ECH waves and whistler mode waves respectively, although the pancakes in this region show no clear evolution as a function of time.

1. Introduction

Highly anisotropic electron pitch angle distributions were first observed in the energy range $50 < E < 500$ eV by GEOS 1 and GEOS 2 [*Wrenn et al.*, 1979]. These distributions were named "pancakes" since they were peaked at 90° to the magnetic field. They were detected over a range of L shells from just outside the plasmapause to geostationary orbit. In addition, evidence was also found for pancakes at energies of a few keV in the higher energy electron experiment on GEOS 1 and 2 [*Horne et al.*, 1987]. Since pancake distributions are highly anisotropic, they are only detected close to the magnetic equator. On the dayside magnetosphere, strong class III electrostatic electron cyclotron harmonic (ECH) waves are also confined to within a few degrees of the magnetic equator [*Gough et al.*, 1979], suggesting that pancakes and ECH waves are related. An attempt to correlate ECH waves with pancake distributions for a period of 7 days at geostationary orbit found that a high anisotropy combined with an absence of dense plasma density generally corresponded with strong ECH waves [*Wrenn et al.*, 1979]. Thus it was suggested that pancakes are the result of pitch angle diffusion driven solely by ECH waves [*Gough et al.*, 1979]. This idea was supported by theoretical studies which modeled experimental electron data and showed that ECH waves driven by a loss cone distribution resonate with electrons from a few hundred eV up to a few keV, that is over the same energy range where pancakes are observed [*Rönnmark and Christiansen*, 1981; *Horne et al.*, 1981, 1987].

[1]Mullard Space Science Laboratory, University College London, Homlbury St Mary, Surrey, England.

[2]British Antarctic Survey, Natural Environment Research Council, Cambridge, England.

[3]Deceased May 28, 1999

[4]Department of Physics and Astronomy, University of Iowa, Iowa City.

Paper number 2000JA900010.
0148-0227/00/2000JA900010$09.00

It was originally thought that since whistler mode waves interact primarily with electrons > 10 keV they would be ineffective at scattering ~ keV electrons [*Kennel et al.*, 1970]. However, it has been pointed out that there is no threshold energy for whistler mode resonance and thus these waves can interact with ~ keV electrons [*Johnstone et al.*, 1993]. The early pitch angle diffusion calculations for whistler mode waves interacting with > 20 keV electrons at $L = 4$ show that whistler mode waves can form pancake distributions at high energies [*Lyons et al.*, 1972]. This suggests that it may be possible for whistler mode waves to form pancake distributions at lower energies and larger L shells under appropriate conditions. On the other hand, new pitch angle diffusion calculations show that ECH waves can form pancake distributions when the wave frequency lies between $(n+\frac{1}{2})$ and $(n+1)f_{ce}$ [*Horne and Thorne*, 2000]. Recent observations from the CRRES spacecraft confirm that pancakes extend up to energies of a few keV and that whistler mode and ECH waves are associated with pancakes [*Meredith et al.*, 1999]. However, which of these two wave modes is more effective for producing pancake distributions has yet to be firmly established.

The fact that pancake distributions are observed at energies up to a few keV may have important consequences as far as the diffuse aurora is concerned. Precipitating electrons at energies of a few keV are believed to be responsible for the diffuse aurora. *Kennel et al.* [1970] originally suggested that ECH waves were responsible for diffuse auroral electron precipitation since they cause precipitation of electrons at energies of a few keV. Furthermore, wave amplitudes of a few mV m^{-1}, which are less than the peak amplitudes observed by *Kennel et al.* [1970], are sufficient to cause strong pitch angle diffusion [*Lyons*, 1974]. However, *Belmont et al.* [1983] found that the fraction of time that ECH waves were detected at geostationary orbit with amplitudes large enough to cause strong diffusion, and hence power the diffuse aurora, was too small. They suggested that some other mechanism must be operative. This suggestion has raised some controversy [*Lyons*, 1984; *Belmont et al.*, 1984] which remains unresolved. Since there is both experimental and theoretical evidence for pancake distributions being the result of pitch angle diffusion and loss, then by studying the formation of pancakes it may be possible to identify the dominant wave mode responsible for the diffusion and hence identify the dominant mechanism responsible for the diffuse aurora.

Observations show that pancake distributions develop from electron distributions which are nearly isotropic in velocity space following substorm injection, on a timescale that is greater than 2 hours [*Meredith et al.*, 1999]. These results were based on a study that identified the onset of particle injections from sudden increases in the electron differential number flux observed by the low energy plasma analyser (LEPA) on board the CRRES spacecraft. In this paper we examine the temporal evolution of the wave amplitudes and the particle distributions following substorm injection using the AE index to determine the time for particle injection. This enables us to present more accurate measurements of the timescales for wave decay and pancake development, to see whether there is a correlation between the time evolution of the waves and pancakes and to set tighter constraints on the particle diffusion rates required for their formation.

The CRRES instruments relevant to this study are briefly described in section 2. In section 3 the behavior of the AE index during injection events is compared with changes in the electron density measurements made by LEPA to establish a value of AE to identify injection events. In section 4 the behavior of the ECH and whistler mode wave amplitudes is examined as a function of time since injection at the nominal equator determined from the field model. The effects of modeling errors on the location of the magnetic equator are considered in section 5. In section 6 the temporal evolution of the pancake index following substorm injection is examined to see if there is a relationship between wave decay and pancake formation. In section 7 the temporal evolution of the development index is examined to help identify the dominant wave mode responsible for pancake formation. The results of this study are discussed in section 8, and the conclusions are presented in section 9.

2. Instrumentation

CRRES was launched on July 25, 1990. The satellite operated in a highly elliptical geosynchronous transfer orbit with a perigee of 305 km and an apogee of 35,768 km. The orbital period was 9 hours 52 min, and the initial apogee was at a magnetic local time of 0800 MLT.

The particle data used in this study were collected by the low energy plasma analyser (LEPA) instrument on board the CRRES spacecraft. This instrument consisted of two electrostatic analyzers with microchannel plate detectors, each with a field of view of 120° × 5°, one measuring electrons and the other ions in the energy range 100 eV < E < 30 keV. The analyzers were mounted on the spacecraft with the 120° range covering angles from 30° to 150° with respect to the spacecraft spin axis, the total range being divided into 15 zones 8° wide. The energy was swept, and not stepped, through the complete range 64 times per spin, synchronized to the spin period of 30 s. The instrument detected the complete pitch angle range from 0° to 180° every 30 s with a resolution of 5.625° × 8° at all energies in the range 100 eV < E < 30 keV. Further details of the LEPA instrument are given by *Hardy et al.* [1993].

The wave data used in this study were provided by the plasma wave experiment on board the CRRES spacecraft. This experiment provided measurements of electric fields from 5.6 Hz to 400 kHz and magnetic fields from 5.6 Hz to 10 kHz with a dynamic range covering

a factor of at least 10^5 in amplitude [*Anderson et al.*, 1992].

The sweep frequency receiver covered the frequency range from 100 Hz to 400 kHz in four bands with 32 logarithmically spaced steps per band, the fractional step separation, df/f being about 6.7% across the entire frequency range. Band 1 (100 to 810 Hz) was sampled at one step per second with a complete cycle time of 32.768 s. Band 2 (810 Hz to 6.4 kHz) was sampled at two steps per second with a complete cycle time of 16.384 s. Band 3 (6.4 to 51.7 kHz) and band 4 (51.7 to 400 kHz) were each sampled 4 times per second, with complete cycling times of 8.192 s. The nominal band widths in each of the four bands were 7 Hz, 56 Hz, 448 Hz, and 3.6 kHz respectively.

3. Determination of the Time Since the Previous Particle Injection

In a previous study of pancake distributions the onset of a particle injection was identified from the sudden increase in the electron differential number flux observed by the LEPA instrument [*Meredith et al.*, 1999]. However, this technique could only identify the injections which occurred when the CRRES spacecraft was outside the plasmapause on the nightside of the Earth. Moreover, in the vicinity of the plasmapause it is often difficult to distinguish between an increase in the electron flux associated with an injection event and that due to the spacecraft moving from the plasmasphere into the plasma sheet where the flux of ~ keV electrons is much higher. In this section an alternative method of identifying particle injections which overcomes these difficulties is investigated.

Dispersionless particle injections have long been used as characteristic signatures of the substorm expansion onset phase [*Arnoldy and Chan*, 1969]. Other signatures include magnetic bays [*McPherrron et al.*, 1973], increases in the *AE* index [e.g., *Sauvaud and Winckler*, 1980], midlatitude Pi2 pulsations [e.g., *Yeoman et al.*, 1994] and VLF chorus events [*Smith et al.*, 1996]. In this paper the *AE* index is used as an independent signature of particle injection since it is readily available at 1 min time resolution and, unlike spacecraft, is not restricted to point measurements which may miss some injections. Variations in the hot plasma electron number density $n_{e,\mathrm{hot}}$ measured by the LEPA instrument on CRRES are first compared with variations in the *AE* index to test this method and establish a threshold level for injections.

The value of $n_{e,\mathrm{hot}}$ is determined from the zero-order moment of the measured electron phase space density $f(\mathbf{v})$ over the energy range 100 eV $< E <$ 30 keV,

$$n_{e,\mathrm{hot}} = \int f(\mathbf{v}) d\mathbf{v}. \quad (1)$$

The lower limit of 100 eV omits variations in the cold plasma density which may also be present. Two criteria are invoked in order to identify an injection event in the particle data. First, $n_{e,\mathrm{hot}}$ should increase by a factor of 2 or more so that only those events which stand out well above any minor fluctuations and noise are included. Second, events occurring near the plasmapause, as identified from the plasma wave data, are rejected since they may correspond to boundary crossings of the plasma sheet. As an example, data for orbit 428, calculated at a 5-min time resolution are plotted as a function of universal time (UT) in Figure 1a. The initial rise in $n_{e,\mathrm{hot}}$ at approximately 1600 UT occurs near the outbound crossing of the plasmapause and is therefore not identified as an injection event. The inbound plasmapause crossing occurs near 2200 UT. The sudden increase in $n_{e,\mathrm{hot}}$ of approximately 3.5 between 1955 and 2035 UT, when the spacecraft was moving from $L = 6.49$ at 0105 MLT to $L = 6.17$ at 0129 MLT, is identified as an injection event. Provisional *AE* indices

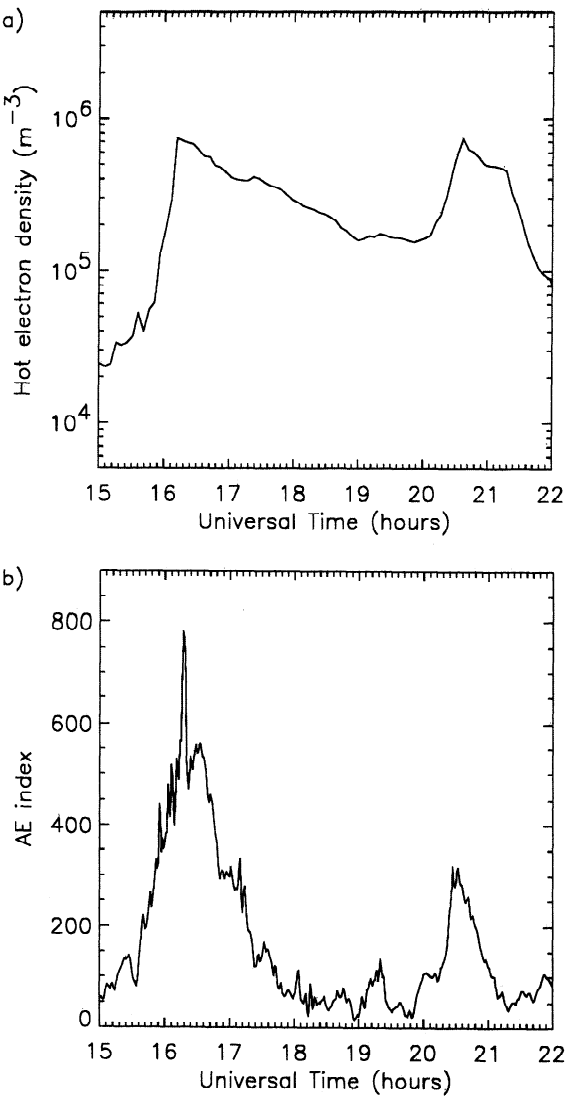

Figure 1. (a) The hot number density as a function of UT and (b) the *AE* index as a function of UT time for orbit 428.

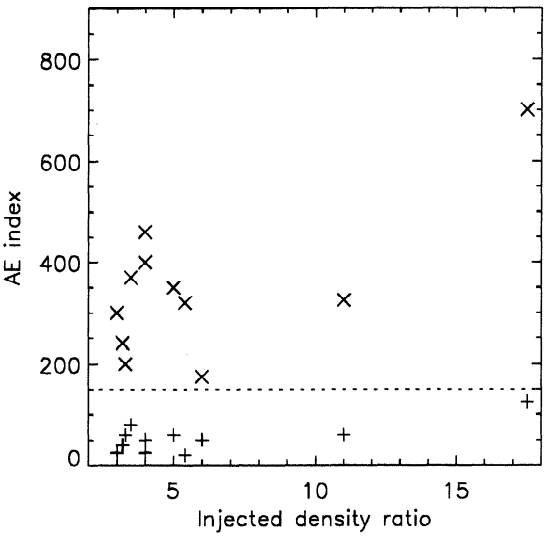

Figure 2. The *AE* index as a function of the injection ratio. The plusses and crosses represent the *AE* index preinjection and postinjection, respectively.

for this orbit are plotted at a 1-min time resolution in Figure 1b. The large increase in *AE* between 2015 and 2035 UT correlates very well with the increase in $n_{e,\mathrm{hot}}$ measured by CRRES. The very large increase in *AE* at approximately 1600 UT shows that an injection event took place at the same time as the spacecraft was transiting the plasmapause. This illustrates an important advantage of using the *AE* index to measure the time of the injection.

Eleven injection events were identified by this method from the 38 orbits used in the original study by *Meredith et al.* [1999]. In Figure 2 the preinjection and postinjection *AE* index is plotted as a function of the injected density ratio, I, given by

$$I = \frac{n_{e,\mathrm{post}}}{n_{e,\mathrm{pre}}}, \qquad (2)$$

where $n_{e,\mathrm{pre}}$ and $n_{e,\mathrm{post}}$ are the hot plasma electron number densities defined by (1) preinjection and postinjection, respectively. The 11 injection events identified in the particle data are all associated with significant increases in the *AE* index. The preinjection and postinjection *AE* indices lie in the range 20 nT $< AE_{\mathrm{pre}} <$ 125 nT and 175 nT $< AE_{\mathrm{post}} <$ 700 nT, respectively. Therefore for the purposes of this paper an injection event is defined as occurring when the *AE* index rises above 150 nT. This should provide a more reliable method of identifying injection events than increases in $n_{e,\mathrm{hot}}$ which are subject to boundary crossings and the limitation of point measurements.

Since injection events last for a finite amount of time and can occur in close temporal proximity such that the next particle injection occurs before the *AE* index has fallen to "quiet" levels, a more realistic parameter for these studies is the time since the end of the previous injection (henceforth referred to as the time since injection). Therefore for the purposes of this study an injection event is said to end when the *AE* index falls from its elevated values observed during particle injections to below 150 nT.

4. Statistical Survey of Wave Amplitudes Close to the Nominal Equator

The temporal evolution of the whistler mode and ECH wave amplitudes following an injection event is first investigated using data from the CRRES plasma wave experiment. We start with the events used in the initial survey, which occurred close to the nominal equator as detailed by *Meredith et al.* [1999].

The data are initially smoothed using a running 6 min average to take out the beating effects due to differences in the sampling and the spin rate. Whistler mode and ECH wave intensities are then obtained by integrating this averaged wave spectral intensity over the ranges $0.1 < \omega/\Omega_e < 1.0$ and $1.0 < \omega/\Omega_e < 6.0$, respectively, where Ω_e is the electron gyrofrequency. The corresponding wave amplitudes are obtained by taking the square root of the appropriate intensities. The noise levels for the ECH and whistler mode wave amplitudes are of the order of 3×10^{-4} and 5×10^{-4} mV m^{-1} respectively. The location of all of the events considered in this study are plotted as a function of L and MLT in Figure 3. The results may be conveniently classified into two categories depending on L value with the dividing line at $L = 6.0$. The events which occur in the region $6.0 \leq L < 7.0$ are mainly located within ±2.5 hours of magnetic midnight and tend to lie well away from the plasmapause. The events which occur in the

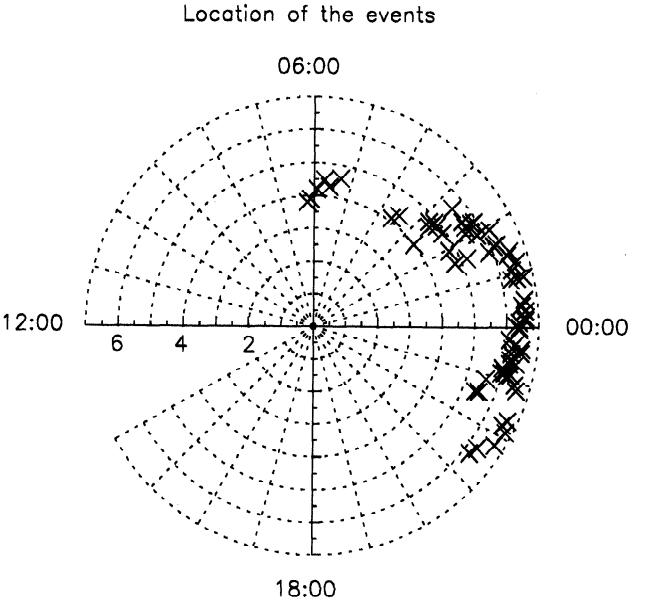

Figure 3. MLT - L shell plot showing where CRRES crossed the magnetic equator. Data from these crossings are used in this study.

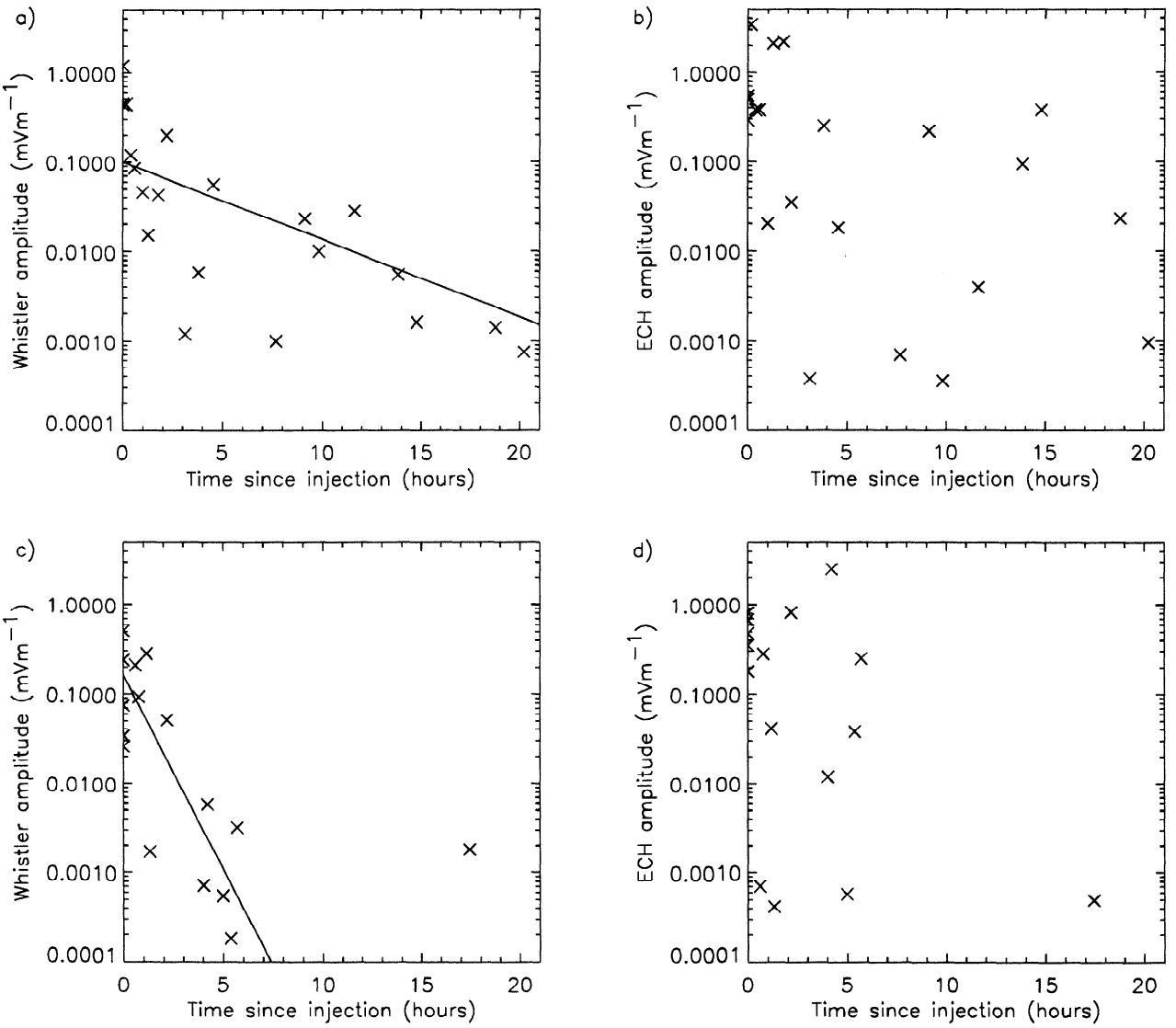

Figure 4. Wave amplitudes from the events used in the original survey, close to the nominal equator, as a function of time since injection. (a) Whistler mode and (b) ECH wave amplitudes for $6.0 \leq L < 7.0$ and (c) whistler mode and (d) ECH wave amplitudes for $3.8 \leq L < 6.0$.

region $3.8 \leq L < 6.0$ are mainly located within ± 2.5 hours of 0400 MLT and tend to lie close to the plasmapause. This distribution of events is largely due to the lack of coverage at low L shell in the midnight sector, caused by the powering down of the instruments during the long shadow periods that occurred during this phase of the orbit.

4.1. Wave Amplitudes Observed in the Region $6.0 \leq L < 7.0$

The whistler mode wave amplitude as a function of time since injection in this region is shown in Figure 4a. The whistler mode wave amplitude peaks at the time of injection and then decays. If an exponential decay of the form

$$A(t) = A_0 e^{-t/\tau} \tag{3}$$

is assumed, the best fit to the data gives $A_0 = 0.1 \pm 0.03$ mV m^{-1} and a decay timescale of $\tau = 5.0 \pm 0.7$ hours. Similarly, the ECH wave amplitude also peaks at the time of injection as shown in Figure 4b. However, the ECH wave amplitudes exhibit considerably more scatter than those for the whistler mode and consequently no fit is attempted.

4.2. Wave Amplitudes Observed in the Region $3.8 \leq L < 6.0$

The whistler mode wave amplitude as a function of time since injection in this region is shown in Figure 4c. Assuming that the amplitudes fall off exponentially, the best fit parameters are $A_0 = 0.16 \pm 0.05$ mV m^{-1} and $\tau = 1.0 \pm 0.1$ hours. The timescale is much shorter than that for whistler mode waves in the region $6.0 \leq L < 7.0$. The ECH wave amplitudes are shown in Figure 4d. These data show a considerable amount of scatter and no trend is immediately apparent.

5. Statistical Survey of Wave Amplitudes at the ECH Equator

In the previous section the magnetic equator was obtained from the Olson-Pfitzer field model. However, the field model does not necessarily give the true location of the magnetic equator, and better estimates may be obtained using signatures in the data. For example, ECH waves are confined to within a few degrees of the magnetic equator [*Gough et al.*, 1979] and tend to peak in amplitude at the equator [*Paranicas et al.*, 1992]. In addition, when pancake distributions are present, the measured particle anisotropy should also peak at the magnetic equator. Therefore the data are reanalyzed using the peak ECH wave amplitude in the vicinity of the nominal equator to identify the magnetic equator (henceforth referred to as the ECH equator) to see whether this significantly affects the results. ECH waves, rather than pancakes, were used to identify the magnetic equator for two reasons. First, pancakes are not always present, and second, observations are more sensitive to the peak in the ECH wave amplitudes than the particle anisotropy due to the resolution of the LEPA instrument.

Equatorial crossings which clearly occurred inside the plasmapause were excluded from the original study. However, in some cases it is difficult to determine the exact location of the plasmapause. An equatorial observation is likely to be inside the plasmapause when a low value of the equatorial ECH wave activity ($A_{ECH} < 0.01$ mV m^{-1}) occurs simultaneously with a high value of the plasma frequency ($f_{pe} > 40$ kHz). Using these criteria, data from three orbits were excluded from the survey at the ECH equator. However, in the survey using the nominal equator, all data points were considered because low values of the ECH wave activity could occur simply because the true equator was missed.

5.1. Wave Amplitudes Observed in the Region $6.0 \leq L < 7.0$

The whistler mode wave amplitude as a function of time since injection in this region is shown in Figure 5a. The best fit to the data gives $A_0 = 0.11 \pm 0.03$ mV m^{-1} and a decay timescale of $\tau = 4.6 \pm 0.7$ hours. These results compare reasonably well with the values obtained close to the nominal equator, showing that whistler mode wave amplitudes are relatively insensitive to the modeling errors in the location of the magnetic equator.

The temporal evolution of the ECH wave amplitudes in this region are shown in Figure 5b. As before, they peak at the time of injection at amplitudes of a few mV m^{-1} and decay with time, but there is much less scatter. The amplitudes decay to a level of the order of ~ 100 μV m^{-1} after a period of 4 - 5 hours and remain at a much higher level than the whistler mode wave amplitudes. The best fit to the data gives $A_0 = 1.9 \pm 0.5$ mV m^{-1} and a decay timescale of $\tau = 6.3 \pm 1.2$ hours.

The average offset between the ECH equator and its nominal position is found to be $1.3° \pm 0.9°$. These results show that the ECH wave amplitudes are very sensitive to the small modeling errors, of the order of 1°, in the location of the magnetic equator.

5.2. Wave Amplitudes Observed in the Region $3.8 \leq L < 6.0$

Whistler mode wave amplitudes in this region are shown in Figure 5c. Assuming that the amplitude falls exponentially the best fit parameters are $A_0 = 0.3 \pm 0.1$ mV m^{-1} and $\tau = 1.1 \pm 0.2$ hours. As before, the timescale is much shorter than that for $6.0 \leq L < 7.0$, but this could be due to the limited range of data.

ECH wave amplitudes in this region are shown in Figure 5d. Again the wave amplitudes peak at injection and there is far less scatter in the data. The best fit to the data gives $A_0 = 2.10 \pm 0.06$ mV m^{-1} and a decay timescale of $\tau = 2.3 \pm 0.6$ hours.

5.3. Wave Excitation

The wave analysis was repeated at the ECH equator using smaller values for the AE threshold to study the effect of smaller substorms on the decay timescales. The AE threshold was first reduced to 100 nT. The decay timescales were found to be $\tau = 8.6 \pm 2.6$ and 4.8 ± 0.9 hours for the ECH and whistler mode wave amplitudes in the region $6.0 \leq L < 7.0$ and $\tau = 1.7 \pm 0.5$ and 0.84 ± 0.12 hours for the ECH and whistler mode wave amplitudes in the region $3.8 \leq L < 6.0$. These results compare favorably with those obtained for a threshold value of 150 nT and show that smaller substorm injections with $100 < AE < 150$ nT do not have a significant effect on the decay timescales. The AE threshold was then reduced to 50 nT but in this case small enhancements of the AE index to values in the range $50 < AE < 100$ nT would meet the criterion for injection events resulting in very small values, of the order of 10 min or less, for the time since injection for most of the events. These are unrealistic values since the average time between substorm events is of the order of 6 hours [*Borovsky et al.*,1993; *Smith et al.*, 1996]. Lowering the threshold to much below 100 nT is thus likely to result in errors.

Since both whistler and ECH wave amplitudes are enhanced at particle injection, this implies that both types of waves are excited by the injection process. The LEPA observations near local midnight show that freshly injected particle distributions are very nearly isotropic in velocity space [*Meredith et al.*, 1999] when averaged over 5 min. This indicates that higher time resolution is required to identify the source of free energy to excite the waves. As the waves grow, they scatter the particles in energy and pitch angle and thus the particle distribution should evolve in time. Therefore it is instructive to consider how the anisotropy of the distribution function at the magnetic equator evolves in time as a measure of wave-induced particle diffusion.

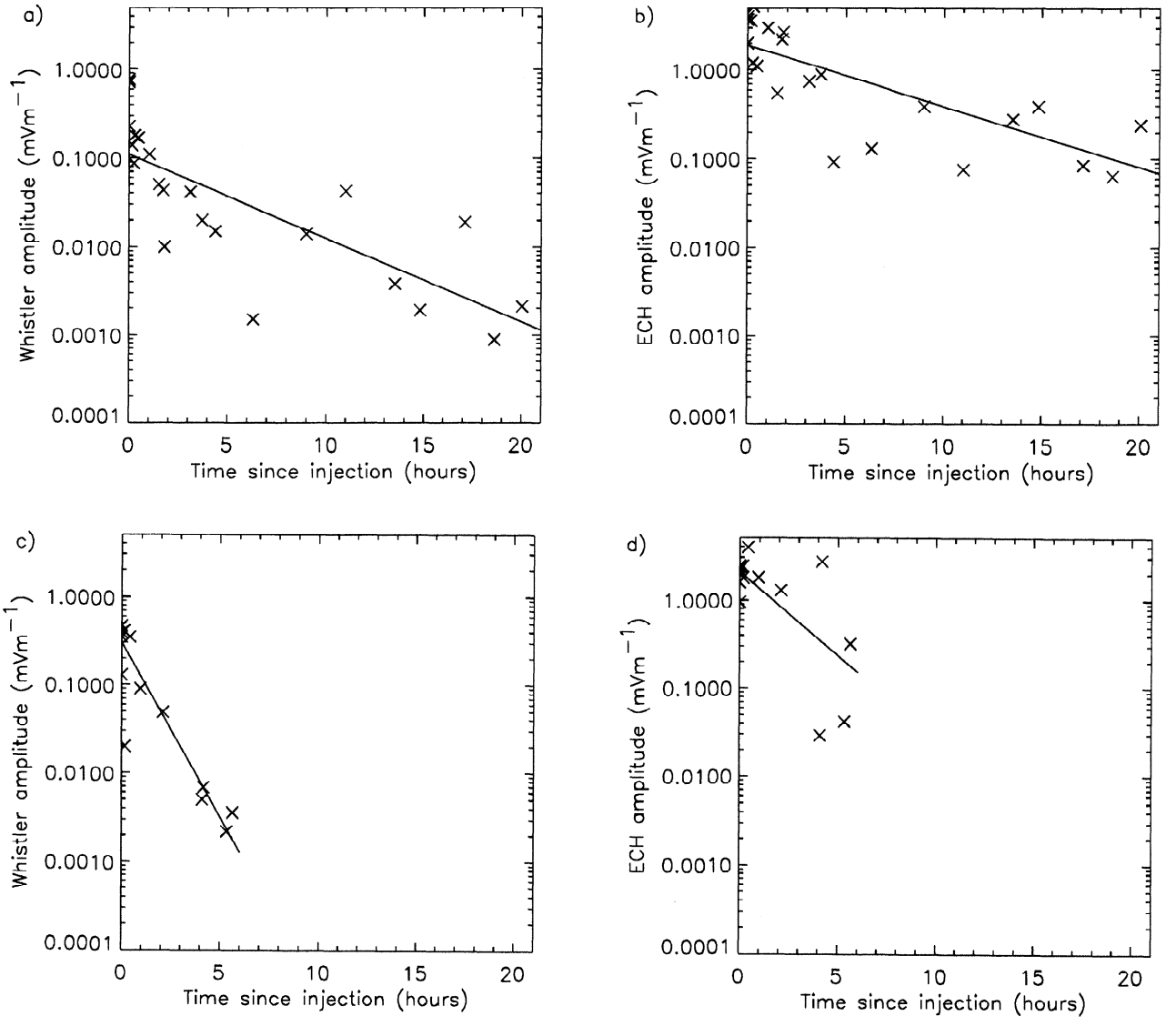

Figure 5. Wave amplitudes at the ECH equator as a function of time since injection. (a) Whistler mode and (b) ECH wave amplitudes for $6.0 \leq L < 7.0$ and (c) whistler mode and (d) ECH wave amplitudes for $3.8 \leq L < 6.0$.

6. Pancake Index

Wrenn et al. [1979] introduced a pancake index, defined as the flux ratio between the 90° and 70° pitch angle, as a measure of the anisotropy of the distrbution function. Here the LEPA data are used to define a similar pancake index PI as follows:

$$PI = \frac{\text{flux at } 90°}{\text{flux at } 67.5°}, \tag{4}$$

67.5° being the closest pitch angle to 70° observed by the LEPA instrument. A measure of the maximum anisotropy for a given distribution is obtained by determining the maximum pancake index $PI_{\max}$ observed over each of the energy sweeps of the LEPA instrument.

The evolution of $PI_{\max}$ as a function of time since injection for $6.0 \leq L < 7.0$ is shown in Figure 6a, with crosses representing values determined from the events used in the original survey close to the nominal equator and diamonds representing values determined at the ECH equator. These results show that the pancake index is relatively insensitive to the modeling errors in the location of the magnetic equator. The maximum pancake index remains low ($PI_{\max} < 3$) for the bulk of the data points for the first 4 hours postinjection. Thereafter the maximum pancake index tends to remain high ($PI_{\max} > 3$), although no clear trend is visible. The 4 hour timescale is consistent with that determined for the decay of both wave types, suggesting that both wave types are involved in the production of pancakes. The results for $3.8 \leq L < 6.0$ are shown in Figure 6b. There is no clear evolution in time, but the data does indicate that more sharply peaked pancakes are possible in this region on much shorter timescales.

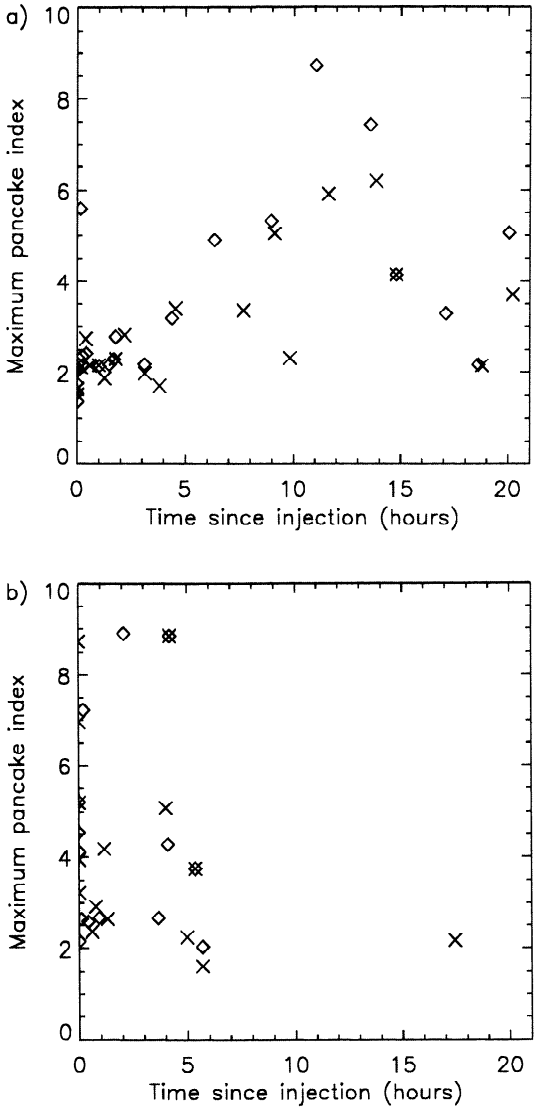

Figure 6. The pancake index as a function of time since injection for (a) $6.0 \leq L < 7.0$ and (b) $3.8 \leq L < 6.0$. The crosses and diamonds represent values determined from the events used in the original survey close to the nominal equator and at the ECH equator, respectively.

7. Development Index

The pancake index does not identify the dominant wave mode responsible for their formation. However, some estimate as to the importance of diffusion by whistler mode waves can be obtained by considering the whistler mode diffusion curves. These curves, which represent the paths followed by the electrons as they diffuse through velocity space under the influence of a broad spectrum of whistler mode waves, have recently been derived by *Summers et al.* [1998] and represent the so-called marginally stable state that develops in the presence of these waves [*Thorne and Horne*, 1996]. The characteristic energy of the plasma E_c is an important scaling factor that determines the shape of the diffusion curves. It is the magnetic energy per particle and may also be expressed in terms of the ratio of the electron gyrofrequency to the electron plasma frequency ω_{pe}:

$$E_c = \frac{B_0^2}{2\mu_0 n_e} = \frac{m_e c^2}{2}\left(\frac{\Omega_e}{\omega_{pe}}\right)^2, \qquad (5)$$

where B_0 is the Earth's ambient magnetic field and n_e is the total plasma density. Following the work outlined by *Meredith et al.* [1999], we fit whistler mode diffusion curves to the equatorial particle distributions to estimate the value of the characteristic energy at each of the equatorial crossings and compare these values with those determined from the plasma wave and magnetometer data. These two independent measures of the characteristic energy enable us to introduce a develop-

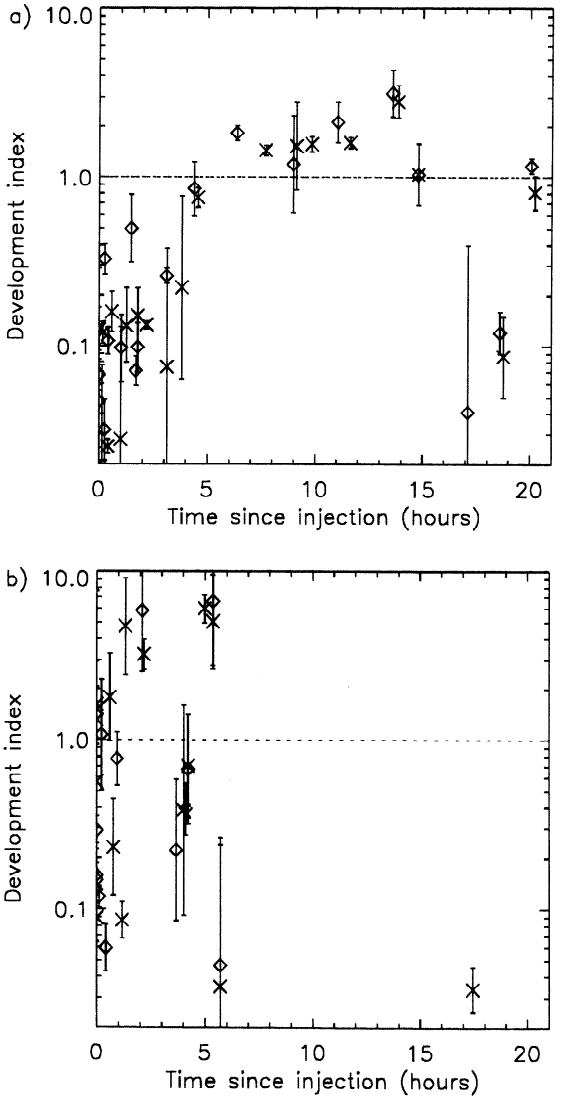

Figure 7. The development index as a function of time since injection for (a) $6.0 \leq L < 7.0$ and (b) $3.8 \leq L < 6.0$. The crosses and diamonds represent values determined from the events used in the original survey close to the nominal equator and at the ECH equator, respectively.

ment index, defined as the ratio of the characteristic energy determined from the particle data to that determined from the plasma wave and magnetometer data, to measure the state of development of a given particle distribution [*Meredith et al.*, 1999]. On this scale a development index of 1 represents a distribution that has reached the marginally stable state. Development indices less than 1 represent developing distributions that are more isotropic in velocity space, and indices greater than 1 represent distributions that have evolved beyond the marginally stable state such as could occur, for example, if other wave-particle interactions are taking place.

The development index is plotted against the time since injection for $6.0 \leq L < 7.0$ in Figure 7a. Crosses represent values determined from the original survey close to the nominal equator and diamonds values at the ECH equator, showing that the development index is relatively insensitive to modeling errors in the location of the magnetic equator. There are clearly two populations. The development index remains low ($D < 0.5$) for all of the distributions observed during the first 4 hours since injection. Thereafter the development index lies in the range $0.8 < D < 3$ for the majority of the data points. There are three anomalous points at $t = 17.1, 18.6$, and 18.8 hours that look like "undeveloped" pancakes suggesting that these distributions have not evolved in the usual way. However, inspection of the AE index during these orbits reveals that it rose to 137, 125, and 125 nT at 5, 71, and 90 min before these events, respectively. These values of AE are not large enough to count as injections using our criterion, but these anomalous data points are most likely due to small injection events. If these anomalous points are excluded, the average value of the development index for the "developed" distributions observed at the ECH equator, which have had more than 4 hours to evolve, is 1.72 ± 0.77. Pancake distributions which lie close to the condition of marginal stability for interaction with whistler mode waves are therefore formed on a timescale of approximately 4 hours.

The development index for $3.8 \leq L < 6.0$ is shown in Figure 7b, showing that there is no clear evolution as a function of time. However, it is interesting to note that pancakes with development indices greater than 5 are common in this region. These distributions are considerably more sharply peaked at 90° than can be predicted by the presence of whistler mode waves alone.

8. Discussion

Whistler mode and ECH wave activity is enhanced at injection over the entire L range covered in this study implying that both wave types are excited by the injection process. Theoretical studies have shown that ECH waves can be excited by a loss cone distribution and whistler mode waves by a temperature anisotropy. However, the injected distributions appear to be isotropic or nearly isotropic in velocity space when measured by the LEPA instrument over a timescale of 5 min. One possibility is that the waves are generated by counterstreaming electron beams, which are often observed for short periods just prior to an isotropic injection. Following injection, a loss cone distribution will naturally form as electrons are lost to the atmosphere and excite ECH waves. However, whistler mode waves are not excited by a very narrow loss cone [e.g., *Swift*, 1981]. Thus the source of whistler mode waves at and following injection is not clear.

The characteristic energy of the plasma at particle injection is very high so that the diffusion curves are very sharply peaked at 90°. Any broadband whistler mode wave activity initially present will lead to diffusion along the diffusion curves from regions of high phase space density to regions of low phase space density. This may lead to diffusion along the curves both into the loss cone region contributing to wave growth and toward the 90° pitch angle contributing to wave decay. The distribution will thus evolve and become more anisotropic until the contours of constant phase space density line up with the diffusion curves. Once formed, and in the absence of any other processes, these marginally stable pancakes would no longer support whistler mode wave growth and whistler mode wave activity would effectively stop.

ECH waves will also be supported at all phases in the growth of the marginally stable pancake while a loss cone distribution is present. Once the marginally stable pancake has formed, the whistler mode wave activity will become very weak. However, the ECH wave activity may continue leading to pancakes that are even more sharply peaked at 90° than could be formed in the presence of whistler mode waves alone. This may be particularly important at lower L and near the plasmapause where the loss cone is larger. More detailed theoretical work, beyond the scope of this present work, would be required to investigate what may happen to a marginally stable distribution in these circumstances.

The average time interval between successive substorm events at geostationary orbit has been measured to be 5.9 ± 6.5 hours with a mode of about 2 to 3 hours [*Borovsky et al.*, 1993]. This is to be compared with an average of 5.5 ± 0.8 hours and a mode of 1.1 hours determined from ground-based substorm chorus events measured at Halley base, Antarctica [*Smith et al.*, 1996]. The differences in modal values are due to the different techniques of measurement and the fact that the ground-based measurements cover a wider region of geospace. In the region $6.0 \leq L < 7.0$ the pancakes are formed on a timescale of approximately 4 hours, which is comparable to the average time interval between successive substorm events. It is therefore likely that these wave-particle interactions are almost continually present in this region leading to the continual supply of electrons to power the diffuse aurora. The results suggest that there should be a modulation in the

intensity of the diffuse aurora observed on ionospheric field lines that map into this region and the intensity would be related to the time since injection.

Fillingim et al. [1999] recently performed a survey of the angular distributions of suprathermal electrons in the energy range 15 eV $< E <$ 200 eV observed by the magnetospheric plasma analyzer on board the geosynchronous satellite 1989-046. The observed distributions were classified as being either field-aligned, trapped, with enhanced fluxes perpendicular to the local magnetic field, both field-aligned and trapped, isotropic or other and were characterized by local time of occurrence and plasma regime. They showed that the two most commonly observed pitch angle distributions in the plasma sheet were trapped and isotropic distributions, consistent with our observations. However, they did not investigate the temporal evolution of the distributions.

9. Conclusions

Data from the wave and particle experiments on CRRES during crossings of the magnetic equator have been used to investigate the evolution of pancake distributions and their relation to ECH and whistler mode wave activity outside the plasmapause. The *AE* index is used to determine the time since the last substorm injection event. The results may be conveniently classified into two categories, events occurring in the region $6.0 \leq L < 7.0$ which are mainly located within ± 2.5 hours of magnetic midnight and tend to lie well away from the plasmapause and events occurring in the region $3.8 \leq L < 6.0$ which are mainly located within ± 2.5 hours of 0400 MLT and tend to lie close to the plasmapause.

The average offset between the magnetic equator determined from the peak ECH wave amplitude and that determined from the field model is $1.3° \pm 0.9°$. The whistler mode wave amplitudes and the indices derived from the particle data are found to be relatively insensitive to these modeling errors. However, the ECH wave amplitudes are very sensitive to the choice of equator. The ECH equator is therefore likely to be a better measure of the true location of the magnetic equator than the nominal equator determined by the field model. Surveys of ECH wave amplitudes should therefore use the ECH equator since greatly reduced and nonrepresentative values are likely to be obtained at the nominal equator.

In the region $6.0 \leq L < 7.0$, pancake distributions develop from injected distributions that are nearly isotropic in velocity space on a timescale of approximately 4 hours. Both ECH and whistler mode wave amplitudes are enhanced during particle injections with typical values in the range $1-5$ and $0.07-0.3$ mV m^{-1}, respectively, and fall off with time since injection. Assuming an exponential time decay ECH and whistler wave amplitudes decay over a timescale of $\tau = 6.3 \pm 1.2$ and 4.6 ± 0.7 hours, respectively. After a timescale of approximately 4 hours the ECH wave amplitudes remain approximately an order of magnitude higher than whistler mode amplitudes. These results suggest that both wave types play a role in the formation of pancake distributions in this region. The whistler mode is likely to be the dominant mode in shaping the final distribution since, once the pancakes have developed, the phase space density contours lie approximately along the characteristic curves for diffusion by whistler mode waves determined independently from the plasma wave and magnetometer data. The fact that the development index exceeds unity in some cases is interpreted as evidence for the presence of other processes, such as wave-particle interactions involving ECH waves. The timescale for pancake production and wave decay is comparable with the average time interval between substorm events so that the wave-particle interactions are almost continually present, leading to a continual supply of electrons to power the diffuse aurora.

In the region $3.8 \leq L < 6.0$ the situation is complicated by the proximity of the plasmapause. The pancakes show no clear evolution as a function of time since injection. Both ECH and whistler mode wave amplitudes are enhanced during particle injections with typical values in the range $1-5$ and $0.1-0.6$ mV m^{-1}, respectively. The timescale for decay is approximately $\tau = 2.3 \pm 0.6$ and 1.1 ± 0.2 hours for ECH waves and whistler mode waves, respectively. Both wave types may play a role in the formation of pancake distributions in this region. However, the pancakes themselves may have much stronger peaks at 90° than predicted by whistler theory, possibly due to strong ECH waves associated with the plasmapause. Therefore it is likely that the ECH waves play the dominant role in shaping the final distribution inside $L = 6.0$, particularly in the vicinity of the plasmapause.

Acknowledgments. We thank the World Data Centre C1 for STP at the Rutherford Appleton Laboratory for providing the *AE* indices used in this paper.

Michel Blanc thanks both referees for their assistance in evaluating this paper.

References

Anderson, R. R., D. A. Gurnett, and D. L. Odem, CRRES plasma wave experiment, *J. Spacecr. Rockets, 29*, 570, 1992.

Arnoldy, R. L., and K. W. Chan, Particle substorms observed at the geostationary orbit, *J. Geophys. Res., 74*, 5019, 1969.

Belmont, G., D. Fontaine, and P. Canu, Are electron cyclotron waves responsible for diffuse auroral electron precipitation?, *J. Geophys. Res., 88*, 9163, 1983.

Belmont, G., D. Fontaine, and P. Canu, Reply, *J. Geophys. Res., 89*, 7591, 1984.

Borovsky, J. E., R. J. Nemzek, and R. D. Belian, The occurrence rate of magnetic substorm onsets: Random and periodic substorms, *J. Geophys. Res., 98*, 3807, 1993.

Fillingim, M. O., M. B. Moldwin, H. K. Rassoul, P. Parrish, M. F. Thomsen, and D. J. McComas, Angular distributions of suprathermal electrons observed at geosynchronous orbit, *J. Geophys. Res., 104*, 4457, 1999.

Gough, M. P., P. J. Christiansen, G. Martelli, and E. J. Gershuny, Interaction of electrostatic waves with warm electrons at the geomagnetic equator, *Nature, 279*, 515, 1979.

Hardy, D. A., D. M. Walton, A. D. Johnstone, M. F. Smith, M. P. Gough, A. Huber, J. Pantazis, and R. Burkhardt, The low energy plasma analyser, *IEEE Trans. Nucl. Sci., 40* (2), 246, 1993.

Horne, R. B., and R. M. Thorne, Electron pitch angle diffusion by electrostatic electron cyclotron harmonic waves: The origin of pancake distributions, *J. Geophys. Res.*, in press, 2000.

Horne, R. B., P. J. Christiansen, M. P. Gough, K. Rönnmark, J. F. E. Johnson, J. Sojka, and G. L. Wrenn, Amplitude variations of electron cyclotron harmonic waves, *Nature, 294*, 338, 1981.

Horne, R. B., P. J. Christiansen, and M. P. Gough, Weak electrostatic waves near the upper hybrid frequency: A comparison between theory and experiment, *J. Geophys. Res., 92*, 3243, 1987.

Johnstone, A. D., D. M. Walton, R. Liu, and D. Hardy, Pitch angle diffusion of low-energy electrons by whistler mode waves, *J. Geophys. Res., 98*, 5959, 1993.

Kennel, C. F., F. L. Scarf, R. W. Fredricks, J. H. Mcghee, and F. V. Coroniti, VLF electric field observations in the inner magnetosphere, *J. Geophys. Res., 75*, 6136, 1970.

Lyons, L. R., Electron diffusion driven by magnetospheric electrostatic waves, *J. Geophys. Res., 79*, 575, 1974.

Lyons, L. R., Comment on "Are equatorial electron cyclotron waves responsible for diffuse precipitation ?", *J. Geophys. Res., 89*, 7589, 1984.

Lyons, L. R., R. M. Thorne, and C.F. Kennel, Pitch angle diffusion of radiation belt electrons within the plasmasphere, *J. Geophys. Res., 77*, 3455, 1972.

McPherron, R. L., C. T. Russel, and M. P. Aubry, Satellite studies of magnetospheric substorms on August 15, 1968 9. Phenomenological model for substorms, *J. Geophys. Res., 78*, 3131, 1973.

Meredith, N. P., A. D. Johnstone, S. Szita, R. B. Horne, and R. R. Anderson, 'Pancake' electron distributions in the outer radiation belts, *J. Geophys. Res., 104*, 12,431, 1999.

Paranicas, C., W. J. Hughes, H. J. Singer, and R. R. Anderson, Banded electrostatic emissions observed by the CRRES plasma wave experiment, *J. Geophys. Res., 97*, 13,889, 1992.

Rönnmark, K., and P.J. Christiansen, Dayside electron harmonic emissions, *Nature, 294*, 335, 1981.

Sauvaud, J.-A., and J. R. Winckler, Dynamics of plasma, energetic particles, and fields near synchronous orbit in the nighttime sector during magnetospheric substorms, *J. Geophys. Res., 85*, 2043, 1980.

Smith, A. J., M. P. Freeman, and G. D. Reeves, Postmidnight VLF chorus events, a substorm signature observed at the ground near $L = 4$, *J. Geophys. Res., 101*, 24,641, 1996.

Summers, D., R. M. Thorne, and F. Xiaio, Relativistic theory of wave-particle resonant diffusion with application to electron acceleration in the magnetosphere, *J. Geophys. Res., 103*, 20,487, 1998.

Swift, D. W., Mechanisms for auroral precipitation: A review, *Rev. Geophys., 19*, 185, 1981.

Thorne, R. M., and R. B. Horne, Whistler absorption and electron heating near the plasmapause, *J. Geophys. Res., 101*, 4917, 1996.

Wrenn, G. L., J. F. E. Johnson, and J. J. Sojka, Stable 'pancake' distributions of low energy electrons in the plasma trough, *Nature, 279*, 512, 1979.

Yeoman, T. K., M. P. Freeman, G. D. Reeves, M. Lester, and D. Orr, A comparison of midlatitude Pi 2 pulsations and geostationary orbit particle injections as substorm indicators, *J. Geophys. Res., 99*, 4085, 1994.

R. R. Anderson, Department of Physics and Astronomy, University of Iowa, Iowa City, IA 52242-1479. (anderson@iowave.physics.uiowa.edu)

R. B. Horne, British Antarctic Survey, Natural Environment Research Council, Madingley Road, Cambridge, CB3 0ET, England. (r.horne@ bas.ac.uk)

N. P. Meredith, Mullard Space Science Laboratory, University College London, Holmbury St. Mary, Dorking, Surrey, RH5 6NT, England. (npm@mssl.ucl.ac.uk)

(Received July 19, 1999; revised January 4, 2000; accepted January 7, 2000.)